Electrothermal Modeling of Surface Acoustic Wave Resonators and Filters

Wolfgang Akstaller, *Student Member, IEEE*, Robert Weigel, *Fellow, IEEE*, and Amelie Hagelauer, *Senior Member, IEEE*

***Abstract*— In this article, an electrothermal modeling approach of surface acoustic wave (SAW) resonators and filters is presented. The starting point for the model is a preliminary design that has to be assessed for thermal aspects. Due to the high geometrical complexity of SAW components, simplifications are elaborated and qualified on resonator and filter levels to prepare the design for thermal simulation. A thermal model is created and simulated in a finite-element method environment. The simulated behavior is exported as a thermal impedance and implemented in a circuit model of a SAW filter. The layout's electromagnetic behavior is taken into account. Electrothermal models of the SAW resonators and the bus bars are developed. The interface to the thermal impedance is achieved by the use of electrothermal ports. The dynamic effect of the frequency shift is included. Verification is done by a comparison of the temperature increase of a resonator in a filter test structure to a corresponding simulation model. The filter is excited by a radio frequency large signal, and the temperature is detected by the use of a resistive temperature sensor. A simulation that shows the impact of mutual heating between the resonators in a filter environment is performed.**

***Index Terms*— Circuit simulation, electrothermal modeling, finite-element method (FEM), surface acoustic wave (SAW) filter, temperature-dependent frequency shift.**

I. Introduction

THE fifth generation of mobile communication networks is planned to enhance the data transfer capability between handheld devices and base stations to the order of magnitude of several gigabits per second. This development is considered to account for the rapidly growing number of data-intensive applications in the consumer market. To achieve this goal, a high order of parallelization of communication channels is needed, which demands a high level of integration of the radio frequency (RF) front end due to limited space in mobile devices [1]. Increased integration in combination with high typical transmit powers up to 26 dBm [2] leads to the necessity to include thermal aspects in the design flow. A particularly crucial part of a mobile phone's front end is the filter section, which includes surface acoustic wave (SAW) filters. Although the temperature-induced frequency shift of the transfer function is lowered by temperature compensation (TC) techniques [3], it is still a challenge [4]. Furthermore, an increased temperature shortens the lifetime [5] and affects the performance of SAW filters.

The ability to precisely predict the behavior of the RF front end components at each operating condition is a crucial aspect in the module design [6], [7]. Therefore, current simulation models of acoustic resonators and filters have to be extended, or new modeling approaches have to be developed in order to include phenomena, such as the local distribution of temperature increase under high-power excitation. Recently, mainly bulk acoustic wave (BAW) filter devices are under investigation in terms of thermal behavior, and corresponding modeling approaches are developed [8]–[15]. There are also studies that relate thermal effects in acoustic resonators to nonlinear electrical behavior [16], [17]. In comparison to BAW devices, the development of a thermal model for SAW resonators and filters is facing different challenges due to a very complex geometrical structure on resonator level including tiny features as well as on filter level where a convoluted routing is typically needed. A phenomenological electrothermal modeling approach is to relate an experimentally determined average temperature increase of a SAW filter to the corresponding input power, which results in a single thermal resistance model [18]. This approach can be extended to separately describe the thermal behavior of each SAW resonator in a filter topology by an individual thermal resistance [19]. Naturally, these models can be extracted as soon as the device is manufactured, which contradicts the demand for a tool for the initial design. A detailed review of a typical SAW resonator and filter manufacturing processes and technology is mandatory to develop a design based electrothermal simulation model of a SAW filter. Such a model can then be applied to investigate the SAW filter's behavior under large-signal conditions and can be utilized to effectively optimize its layout. In SAW resonators, the acoustic waves are excited by a periodic metallic electrode structure with alternating polarity. This basic structure is the interdigital transducer (IDT). By adding reflectors at the ends of the IDT, a resonator is created. As this is the basic component of a filter, sufficient effort has to be spent on the implementation

Manuscript received March 31, 2020; accepted May 28, 2020. Date of publication June 2, 2020; date of current version October 26, 2020. *(Corresponding author: Wolfgang Akstaller.)*

Wolfgang Akstaller and Robert Weigel are with the Institute for Electronics Engineering, Friedrich-Alexander University Erlangen-Nuremberg, 91058 Erlangen, Germany (e-mail: wolfgang.akstaller@gmx.de).

Amelie Hagelauer is with the Chair of Communications Electronics, University Bayreuth, 95447 Bayreuth, Germany.

Digital Object Identifier 10.1109/TUFFC.2020.2999545

This work is licensed under a Creative Commons Attribution 4.0 License. For more information, see https://creativecommons.org/licenses/by/4.0/

of a thermal model. The electrodes are attached to metallic bus bars corresponding to their polarity. Several resonators are connected by routing layers in order to realize a SAW filter. Furthermore, passivation layers are utilized. The RF currents are routed through the metallic bus bars and electrodes. They not only lead to a dissipation of power but also are significant heat paths and, therefore, need particular attention in the modeling process. The multitude of different layers and small geometric objects demand a stepwise modeling approach.

This article is focusing on the key findings and elaborated approaches for the development of an electrothermal model of SAW devices. Furthermore, it includes an experimental validation and presents additional simulation capabilities. In Section II, the modeling approach for the IDT is covered, and Section III describes the transition to the whole filter layout. Both modeling steps are done in a finite-element method (FEM) environment. Section IV is dedicated to the implementation of the electrothermal model in a circuit simulator. Sections V and VI cover the model verification and a simulation of a resonator's temperature increase due to mutual heating within the filter layout. The following section describes the modeling approach at the resonator level.

II. Thermal Modeling of a SAW IDT

An FEM approach is eligible to determine the thermal behavior of the SAW resonator's IDT. In the presented approach, heat conduction is considered to be the dominating effect. Convection is neglected due to the relatively small size of the SAW devices, and thermal radiation is not taken into account because of the relatively low maximum temperatures. The boundary conditions in the simulation model have to be chosen to represent a realistic scenario. This can be a SAW component that is soldered in flip-chip technology onto a printed circuit board (PCB) and sealed with epoxy. The soldered connection is usually a good heat path and can be modeled as thermal ground. In this article, the validation of the model uses an on-wafer SAW device, and the model has to be prepared accordingly. The wafer chuck is an excellent thermal ground. Thus, the thermal ground condition is considered at the bottom of the substrate of the model. In the lateral direction, a perfectly matched layer is applied to represent the large wafer. Nonetheless, the thermal modeling approach is not restricted to this setting but can be used to generate a resonator model that is situated in a complex thermal environment.

The high complexity of the electrode structure demands the development of geometric simplifications. The approach is to represent the complex electrode structure by a thermal equivalent circuit that can be simplified and modeled by an equation for each spatial direction. The result is a uniform geometrical layer that represents the same macroscopic behavior as a model with structured electrodes. To develop an effective thermal model of the IDT area, a 2-D periodic model is examined. A drawing of the model is shown in Fig. 1.

The model consists of an electrode and a substrate. It is designed to represent a periodic electrode structure in the lateral direction (x-direction). The periodic boundary conditions (PBC) are applied on the left- and right-hand sides of the substrate. Thus, an infinite repetition of the model's behavior is achieved in the x-direction.

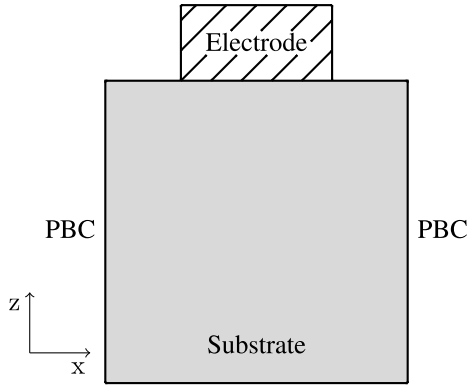

Fig. 1. Periodic 2-D model of a single electrode to represent the IDT. PBCs are applied on the sides of the substrate. The drawing is not to scale.

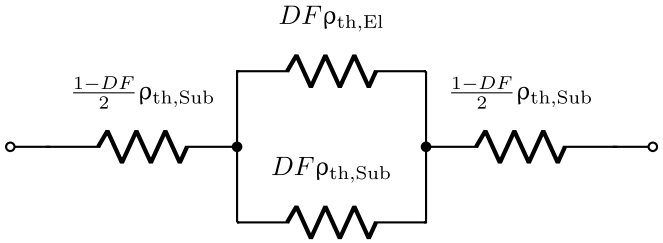

Fig. 2. Thermal equivalent circuit to determine the specific thermal resistance $\rho_{\mathrm{th},x}$ of the periodic IDT model in the x-direction.

A. IDT's Equivalent Specific Thermal Conductivity in the X-Direction

To simplify the IDT area of a resonator, an equivalent description that models the thermal behavior by an anisotropic equivalent layer is elaborated. Therefore, all three spatial directions have to be treated separately. The thermal equivalent circuit of the periodic IDT model to describe the thermal behavior in the x-direction or propagation direction of the acoustic waves $\rho_{\mathrm{th},x}$ is shown in Fig. 2.

In the equivalent circuit, four elements are used to represent the different sections of the periodic model. The areas in the x-direction without the electrode (free substrate) are described by the specific thermal resistance of the substrate $\rho_{\mathrm{th,Sub}}$. The duty factor (DF) is the ratio of metalized to free area. Normalization to the DF is applied, which is used as a modeling parameter. The part that is covered by the metallic electrode is described by a parallel circuit of $\rho_{\mathrm{th,Sub}}$ and the specific thermal resistance of the electrode $\rho_{\mathrm{th,El}}$. Again, the values are normalized to the fraction of the area using the DF. The circuit can be described by the following equation:

$$\rho_{\mathrm{th},x} = \frac{1-\mathrm{DF}}{2}\rho_{\mathrm{th,Sub}} + (\mathrm{DF}\rho_{\mathrm{th,El}}) \parallel (\mathrm{DF}\rho_{\mathrm{th,Sub}}) + \frac{1-\mathrm{DF}}{2}\rho_{\mathrm{th,Sub}}. \quad (1)$$

The specific thermal conductivity is calculated as the reciprocal value of the specific thermal resistance. Thus, the specific

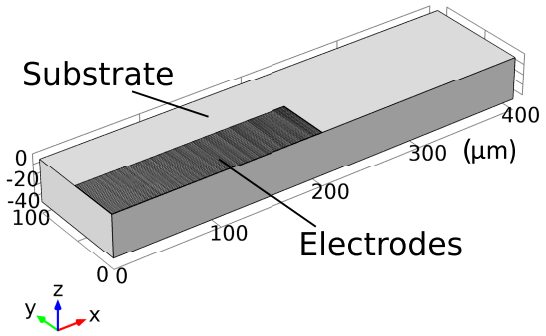

(a) Model with 3D implemented electrodes.

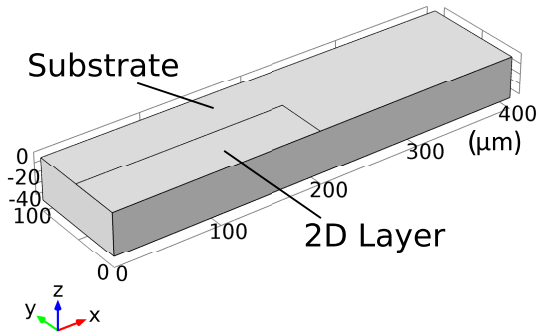

(b) Model using equivalent layer for electrodes.

Fig. 3. Simulation models to validate the approach that represents a 3-D IDT by a 2-D layer, which is implemented with anisotropic thermal properties. (a) Model with 3-D implemented electrodes. (b) Model using equivalent layer for electrodes.

thermal conductivity in the x-direction κ_x is calculated by the following equation:

$$\kappa_x = \frac{\kappa_{\mathrm{Sub}}(\kappa_{\mathrm{El}} + \kappa_{\mathrm{Sub}})}{\kappa_{\mathrm{El}} - \mathrm{DF}\kappa_{\mathrm{El}} + \kappa_{\mathrm{Sub}}} \tag{2}$$

in which the specific thermal conductivities of the substrate κ_{Sub} and the electrode κ_{El} are used.

B. IDT's Equivalent Specific Thermal Conductivity in the Y- and Z-Directions

In the direction along the electrode fingers (y-direction, see Fig. 3), the specific thermal conductivity is calculated by the ratio of metalized to unmetalized area. This can be seen as a parallel circuit of metal electrode and substrate material. The following equation describes the ratio:

$$\kappa_{\mathrm{y}} = ((1 - \mathrm{DF})\kappa_{\mathrm{Sub}})||(\mathrm{DF}\kappa_{\mathrm{El}}). \tag{3}$$

In terms of thermal conductivity, the electrode dominates the behavior, and 3 is approximated by

$$\kappa_{\mathrm{y}} \approx \mathrm{DF}\kappa_{\mathrm{El}}. \tag{4}$$

The specific thermal conductivity in the height of the model (z-direction) is also described by a parallel circuit of thermally highly conductive material and a weakly conductive material. Thus, the latter can be neglected, and the specific thermal conductivity in the z-direction is calculated by

$$\kappa_{\mathrm{z}} \approx \mathrm{DF}\kappa_{\mathrm{El}}. \tag{5}$$

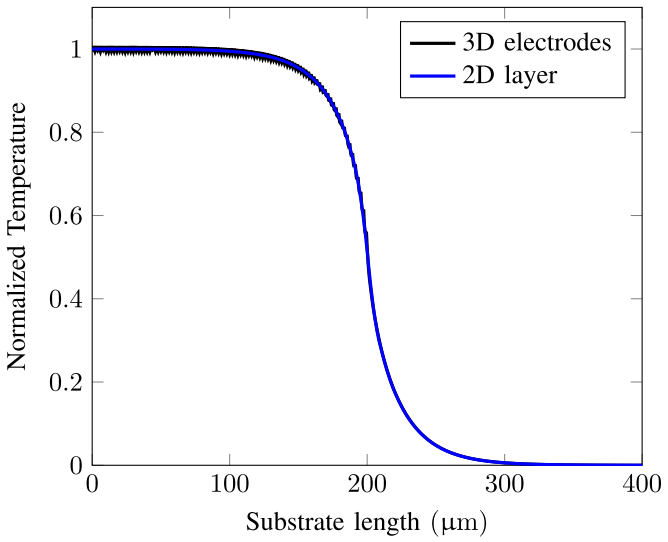

Fig. 4. Simulated temperature increase at an IDT to validate the approach to model 3-D structured electrodes by a 2-D layer with anisotropic thermal properties. The metallization ratio is DF $= 0.5$, and the temperature increases are normalized to the maximum temperature in the model, including the 2-D layer approach.

C. Validation of the Equivalent Model in a 3-D Simulation

To validate the approach of using a 2-D uniform equivalent layer to represent the IDT area, two thermal simulations are performed. Two different models, one with 3-D structured electrodes and the other one using the determined equivalent anisotropic thermal properties, are created. The elaborated models are shown in Fig. 3.

Both models have a substrate length of 400 μm (x-coordinates), a width of 100 μm (y-coordinates), and a height of 50 μm (z-coordinates). The model, which is shown in Fig. 3(a), features 100 electrodes modeled as 3-D elements with DF $= 0.5$. This results in an electrode width of 1 μm. The electrodes are designed to have a length of 50 μm and a height of 0.3 μm. The second model, which is shown in Fig. 3(b), is defined with the same substrate dimensions but includes a 2-D layer to represent the electrodes. The 2-D layer is implemented to represent the same thermal behavior as the electrode structure using the approach described in the previous section. The metallic 3-D electrodes and the equivalent 2-D layer are each heated with the same input power. The simulated temperature responses are evaluated along the substrate edge at $y = 0$ μm and $z = 0$ μm and are shown in Fig. 4.

The simulated responses show excellent agreement. Along a substrate length up to 200 μm, a wobble is observed in the simulation model, including the 3-D electrodes due to the temperature distribution in the electrodes. This effect is not considered in the 2-D layer, but, as it has an amplitude of 0.6% of the total temperature, it can be neglected.

III. Thermal Modeling of SAW Filters

A SAW filter topology usually consists of several series and shunt resonators. These are connected to each other by metallic bus bars. The shunt elements share a ground area. The

TABLE I
POSSIBLE LAYER COMBINATIONS OF A TCSAW LAYER STACK. THE AREAS ARE LISTED AS FRACTIONS OF THE FILTER TEST STRUCTURE'S TOTAL AREA

	RT1/SL/RT2	RT1/OX/RT2	IDT/RT2	OX/RT2	IDT	OX
RT2 (Routing Layer 2)	X	X	X	X		
Oxide Layer		X	X	X	X	X
SL (Oxide Opening)	X					
IDT			X		X	
RT1 (Routing Layer 1)	X	X				
Fraction of area	12 %	2.0 %	0.20 %	19 %	35 %	31.8 %

routing dimensions are significant and need to be considered in a thermal simulation model. To reduce the complexity of the layout and to simultaneously model different layers in a simulation model, an approach to combine certain layers is elaborated. First, a segmentation of the layout is introduced.

A. Layout Segmentation

The SAW filter structure is manufactured by processes similar to that in the conventional semiconductor industry. Naturally, the different functional layers are deposited individually. This leads to a layer stack with a high aspect ratio and relatively low thickness. The layout of the examined SAW filter consists out of several thermally significant layers. Similarly, thermally negligible layers are not considered in the presented approach. The piezoelectric substrate is the base of the structure. The IDT, which thermal properties are discussed in Section II, is the location of electrical and mechanical interaction. It is deposited as a metallic layer, which is also used as the lower routing layer (RT1) that provides an electrical connection between the different resonators. To achieve electrical isolation between the IDT and RT1 toward higher layers, a passivation layer that consists of silicon dioxide (SiO_2) is used. Furthermore, it is applied as a means to control the temperature coefficient of frequency (TCF) of the resonators. The oxide layer (OX) provides low thermal conductivity. A sacrificial layer (SL) is used to define openings in the oxide layer. The openings are used to establish electrical contact of the lower RT1 to a higher routing layer (RT2). On top of that, a housing structure is implemented out of photoresist, and metallic vias are manufactured in order to provide electrical contact to the filter.

The substrate, housing, and vias are considered as large and plane objects in the elaborated modeling approach and, thus, are implemented as 3-D objects without further simplification, whereas the other mentioned layers have to be simplified. From the above, the layout is subdivided into several zones in which certain layer combinations are possible. The combinations are listed in Table I.

The largest area (35%) is covered by the IDT layer, which is followed by the OX layer with 31.8%. The IDT layer as the active area has a strong impact on the temperature distribution. The area in which the upper routing layer overlaps the oxide (OX/RT2) is 19% of the filter test structure's area. This layer also significantly contributes to the temperature distribution due to the high conductivity of the metal in RT2. The remaining combinations RT1/SL/RT2, RT1/OX/RT2, and

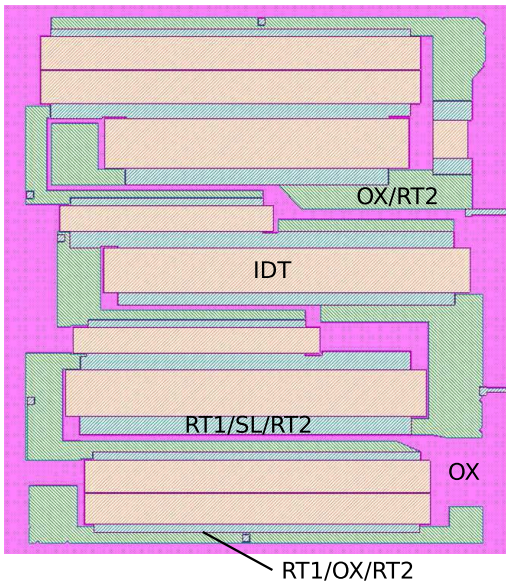

Fig. 5. Schematic layout of a filter test structure after layout segmentation. Five different layer combinations appear after the layers IDT and IDT/RT2 are merged. This approach enables an efficient simulation in FEM.

IDT/RT2 cover 12%, 2%, and 0.2%, respectively. The combinations RT1/SL/RT2 and RT1/OX/RT2 impact the temperature distribution because of the proximity to the main heat source (IDT layer) as well as the high thermal conductivity due to the metallic routing layers. To avoid too small objects and due to the low fraction of the total layout, the layer IDT/RT2 is merged in the model with the IDT area. Fig. 5 shows a schematic representation of the different layer combinations after the segmentation and simplification processes.

The segmented layout is used to simplify the simulation model. Each combination has up to three different layers and can be treated as a single object. The thermal properties are therefore modeled by an equivalent layer, which is calculated in an additional simulation. Furthermore, due to the relatively low physical height, the segmented layout is implemented as a 2-D layer in the 3-D model. This approach significantly reduces the complexity of the structure and, thus, enables simulation in FEM, while it maintains the thermal behavior of the real device.

B. Thermal Behavioral Modeling

Similar to the electrical impedance that describes the behavior of an electrical circuit, a thermal impedance can be defined to express the thermal behavior of a network. Therefore, thermal ports have to be defined at locations where heat is generated and at the model boundaries where inward or outward heat flux has to be considered. The behavior between these thermal ports is described by the complex value of the thermal impedance. The real values correspond to the resistive path, and the imaginary part is able to describe the thermal capacitance. The values are usually arranged as an impedance parameter matrix, and each entry stands for the correlation either between two thermal ports or between a thermal port and the thermal ground. The entries describe

the sum of all heat paths between the two ports in the device. Time-dependent modeling uses the complex thermal impedance values, whereas, in stationary considerations, the thermal resistance is utilized. In this study, the stationary approach is applied. In order to calculate the values, a thermal simulation is run with different load cases. In each load case, a single port is heated by the defined power. The temperature differences at each port to the thermal ground and toward the other ports are related to the input power. Thus, the corresponding entry of the thermal resistance matrix (TRM) is extracted. The diagonal entries of the TRM correspond to the self-heating of the thermal port, and the remaining entries describe the mutual heating. This TRM is then stored as an impedance parameter file and can be implemented in circuit simulators to model the thermal behavior of the device.

IV. Electrothermal Model of SAW Filters

After the TRM is extracted from the thermal simulation, it is implemented in an RF model of the SAW filter. Electrothermal ports (ETPs) are introduced at each active component in the electrical model of the filter. They are the link between the electrical domain and the thermal domain and are connected to the corresponding thermal ports of the TRM. The DC quantities current and voltage in the circuit simulation model, therefore, represent their thermal counterparts' heat flow and temperature.

A. Electrothermal Resonator Model Including Temperature-Dependent Frequency Shift

There are several electrical models that are typically used in SAW resonator modeling, e.g. the coupling of modes (COM) or the modified Butterworth-van Dyke (mBVD) approaches. Here, the chosen variant to model the electrical behavior of the SAW filter is based on the mBVD approach. Thus, the behavior of the individual resonators in the filter layout is described. The resonators are connected to an electrical impedance file, which represents the electromagnetic (EM) behavior between the electrical ports. Consequently, the routing as well as parasitic effects on the chip are considered. The temperature-dependent response of the resonators is captured in the mBVD models. A schematic lumped element circuit of the mBVD model is shown in Fig. 6.

The transfer function of the mBVD model corresponds to a parallel and series resonant circuit. Using the proper selection of the lumped elements, it models the main resonance response of a SAW resonator. The parallel f_p and series f_s resonance frequencies without temperature dependence are calculated in the loss-less model by the following equations:

$$f_s = \frac{1}{2\pi\sqrt{L_m C_m}} \tag{6}$$

$$f_p = \frac{1}{2\pi}\sqrt{\frac{C_m + C_p}{L_m C_m C_p}} = f_s\sqrt{1 + \frac{C_m}{C_p}}. \tag{7}$$

The temperature coefficient of frequency is defined as

$$\mathrm{TCF} = \frac{\Delta f}{f_{\mathrm{nom}}(T - T_0)} \tag{8}$$

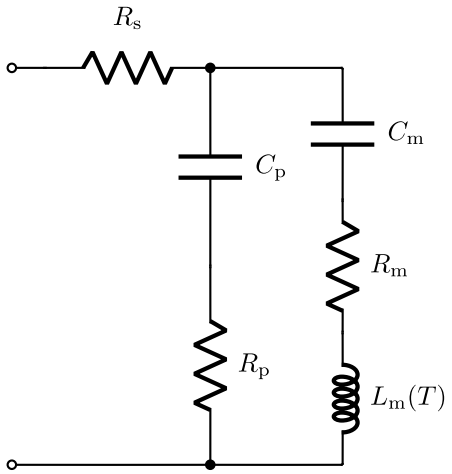

Fig. 6. Modified Butterworth-van Dyke model, including a temperature-dependent inductance to describe the RF response of a SAW resonator.

where the shift in frequency is represented by Δf, the nominal frequency is f_{nom}, and the corresponding difference in temperature is calculated as the difference of the reference temperature T_0 (e.g. room temperature) and the device temperature T. The implementation of a temperature-dependent inductance $L_m(T)$ allows for modeling the shift of frequency response due to changing temperature. A first-order temperature coefficient t_{c1} is used to model the inductance L_m

$$L_m(T) = L_{m,\mathrm{nom}}(1 + t_{c1}(T - T_0)) \tag{9}$$

in which $L_{m,\mathrm{nom}}$ stands for the nominal value of the inductance. Due to the proportionality of f_s and f_p, as shown in 7, a temperature dependence of f_s directly leads to a temperature dependent f_p. Therefore, 6 is extended to incorporate a temperature dependence by applying the first-order temperature coefficient TCF [see 8] similar to 9 [8]

$$f_s(T) = \frac{1 + \mathrm{TCF}(T - T_0)}{2\pi\sqrt{L_m C_m}} = \frac{1}{2\pi\sqrt{\alpha(T)\ L_m C_m}}. \tag{10}$$

In the equation, the nonlinear function $\alpha(T)$ is introduced. It is approximated by a Taylor series up to the second order ($n = 2$) [20]

$$\alpha(T) = \frac{1}{(1 + \mathrm{TCF}(T - T_0))^2} \approx 1 - 2\mathrm{TCF}(T - T_0). \tag{11}$$

The approximated function is fed back into 10

$$f_s(T) = \frac{1}{2\pi\sqrt{\underbrace{(1 - 2\mathrm{TCF}(T - T_0))L_m}_{L_m(T)}\, C_m}}. \tag{12}$$

The resulting temperature dependence is allocated to the temperature-dependent inductance $L_m(T)$. The notation of the temperature dependence is compared to 9. It can be seen that the resulting first-order temperature coefficient is $t_{c1} = -2\ \mathrm{TCF}$. This definition of the $L_m(T)$ is utilized in each individual model of SAW resonator in the electrothermal SAW filter model. It allows for the exact modeling of the filter transfer function under the impact of local heat spots due to a temperature distribution across the filter.

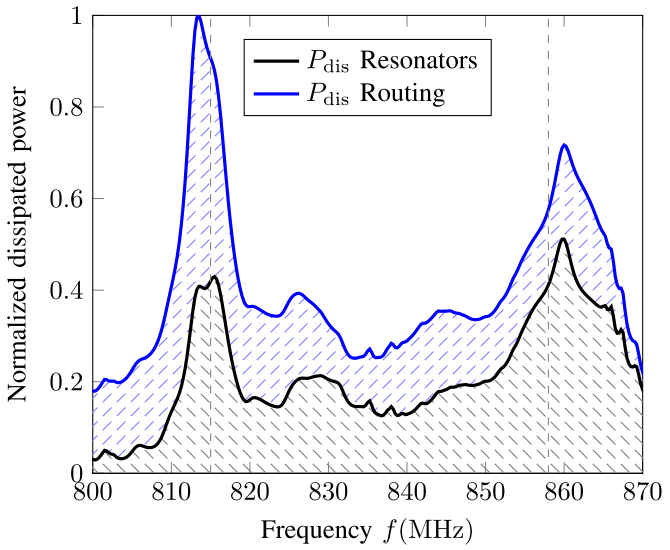

Fig. 7. Simulation of the dissipated power of the filter test structure normalized to the highest value. The simulation is performed under 50-Ω port impedance conditions. The cumulative plot splits up the power into the dissipation in the resonators (black area) and the dissipation in the routing of the filter layout (blue area). The passband of the filter lies between the frequencies 815 and 858 MHz and is denoted with vertical lines.

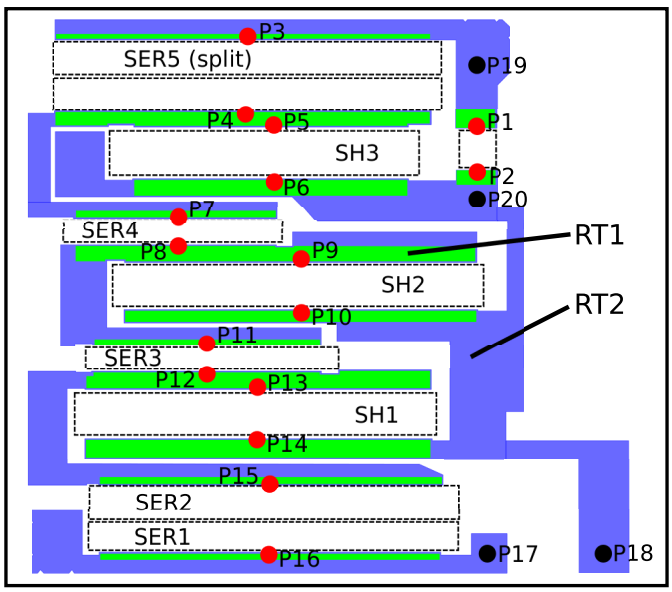

Fig. 8. EM port definitions at the filter test structure. The layout shows the substrate, routing layers RT1 and RT2, and the location of the acoustic resonators (dashed boxes). The filter is designed as a 3.5 stage ladder topology, including five series resonators (SER) and three shunt resonators (SH). The filter input and output ports are marked by dots in black color, and the red dots mark the ports to the acoustic elements. A similar EM simulation model setup is presented in [13].

The electrical losses in the resonator model are described by the resistances in the mBVD model. In SAW resonators, the dissipated power is a combination of the Joule effect, dielectric loss, and mechanical loss [21]. In good approximation, the losses are assumed to directly lead to uniform local heating at the corresponding resonator area. Thus, the electrical losses at R_s, R_m, and R_p are summarized and fed to an ETP [8]. Therefore, the analogy between electrical and thermal quantities is used [22]. The resonator model is then connected via the electrical ports to the EM impedance file and via the ETPs to the TRM.

B. Simulated Influence of the Filter Routing

An electrothermal simulation model of a SAW filter test structure that includes eight resonators is created. The approach that is described earlier is applied. A comparison between the overall dissipated power and the sum of dissipated power at the resonators indicates that a significant amount of losses is not yet considered. The remaining component that is able to dissipate power in the simulation model is the EM impedance file. This experiment leads to the insight that the filter routing acts as an important contributor to the ohmic losses. The dissipated powers in the resonators as well as in the routing are shown in Fig. 7 as a cumulative plot. The simulation is run at an input power of 29 dBm, and the plot is normalized to the maximum loss at the frequency of 813.5 MHz.

Both sources of losses significantly contribute to the total dissipated power across the whole frequency range. At the lower filter skirt, the maximum losses occur at $f = 813,5$ MHz, which are to 59.0% due to the routing. The highest normalized dissipated power above the higher passband edge of 0.72 is observed at a frequency of 860.0 MHz. The impact of the routing to this value is 28.7%. Besides the significant impact of the routing, a further result of this simulation is that the dissipated power due to the filter routing is not constant over the passband frequency range. As a consequence, the routing needs to be considered in an electrothermal model of a SAW filter, and the impact needs to be located at the actual position in the layout. Therefore, individual thermal ports need to be defined in the thermal FEM model to represent the single bus bars. Only this allows for the prediction of accurate temperature distribution across the filter.

C. Electrothermal Modeling of the Filter Routing

The impact of filter routing has to be included in the electrothermal model. Therefore, the lossy behavior of the bus bars that connect to the resonators and to the electrical ground is studied. The aim is to represent each bus bar with an electrothermal model that has a connection via an ETP to the corresponding thermal port in the TRM. Thus, their contribution to the temperature increase at the exact location in the layout is considered in the filter model.

An EM simulation is used to determine the RF behavior of the filter layout without the resonators. Therefore, the filter geometry and the material properties of the substrate and metallic routing are considered. Single-ended ports are defined at the positions of input and output of the filter and the individual resonators. The single-ended port definition is mandatory to obtain a global ground, which is needed to extract the behavior of the individual paths between certain ports in the layout. The ports are defined, as shown in Fig. 8. The validity of defining EM ports in a centered position of the resonators' bus bars is shown in a similar modeling approach for BAW filters [13].

TABLE II
EXCERPT OF THE BUS BAR RESISTANCE MATRIX CORRESPONDING TO THE PORT DEFINITIONS IN FIG. 8

	P1	P2	P3	P4	P5	P6	P7
P1			0.581 Ω				
P2						0.279 Ω	
P3	0.581 Ω						
P4					0.056 Ω		1.268 Ω
P5				0.056 Ω			1.287 Ω
P6		0.279 Ω					
P7				1.268 Ω	1.287 Ω		

To extract the impedance values of the metallic bus bars, the behavior of the EM impedance matrix is simulated between two ports, while the remaining ports are left open. The resulting S-parameter is evaluated with the following equation [23]:

$$Z_{\text{Trans}} = 2Z_0 \frac{1 - S_{21}}{S_{21}} \tag{13}$$

where Z_{Trans} corresponds to the transmission impedance between the assessed ports, Z_0 is the characteristic impedance, and S_{21} is the S-parameter between the two examined ports. This approach is applied to each combination of ports, and in the end, a matrix of all occurring Z_{Trans} is generated. As the values of the bus bar resistance are needed, the physical meaning of the resulting Z_{Trans} has to be checked. The following criteria are used to sort out the values of the Z_{Trans} matrix that does not correspond to a metallic bus bar.

1) $0 < \text{real}\{Z_{\text{Trans}}\} < 10\ \Omega$.
2) $|(\text{imag}\{Z_{\text{Trans}}\})/\text{real}\{Z_{\text{Trans}}\}| < 50$.

The real part of Z_{Trans} corresponds to the ohmic resistance value of the connection between the ports. As the intention is to extract the resistance values of metallic bus bars, only positive entries below 10 Ω are allowed. Every value beyond this value is considered not to be connected via a metallic bus bar. In addition, a second criterion is used in order to sort out highly reactive parasitic elements. Only entries with an imaginary part maximum 50 times as high as the real part are allowed. Any entry that is outside these limits is not assumed to be a lossy bus bar. An excerpt from the resulting values of the SAW filter test structure is shown in Table II.

The EM impedance matrix is reciprocal. Consequently, the bus bar resistance matrix has to be symmetrical, which is the case. Good correspondence of path length and dimension of the bus bars in the layout (see Fig. 8) and the resistance values is observed. The path between the ports P1 and P3 is narrow and of middle length. This results in a resistance value of 0.581 Ω. In comparison, the connection between the ports P2 and P6 is shorter and wider. Thus, the resistance value of 0.279 Ω seems reasonable. The path between P4 and P5 is very short, which results in a very low resistance of 0.056 Ω. The very long distances along the bus bar between P4 and P7 as well as P5 and P7 lead to the high resistance values of 1.268 and 1.287 Ω, respectively. The latter value is slightly higher due to the longer path. These resistance values are used in the electrothermal modeling approach in order to implement the bus bar traces. The exact values of electrical losses that contribute to the heating of the device can be calculated in the correct position in the layout. To further improve the model and to account for local RF current distributions, long bus bar traces, for example, the path between P4 and P7, can be divided into several smaller entities. This needs to be considered in the thermal FEM simulation as additional thermal ports.

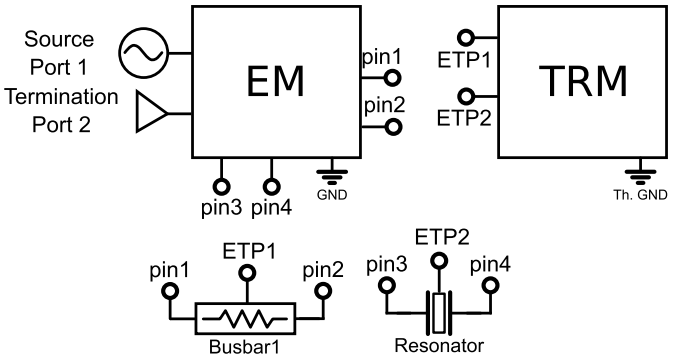

Fig. 9. Schematic of an electrothermal model, including large-signal simulation ports, an EM impedance file to model the RF behavior of the routing and substrate, a TRM that models the thermal behavior of the filter, a bus bar, and a resonator model that describes their RF behavior in the circuit simulation [24].

D. Schematic of the Electrothermal Model

Fig. 9 shows an exemplary schematic of an electrothermal model in which a resonator is connected to a bus bar trace.

The schematic includes a large-signal simulation Port 1 and a termination Port 2. They are directly connected to the EM impedance matrix in which the signal is distributed. The single-ended matrix connects to the bus bar model via pin 1 and pin 2 and to the resonator model via pin 3 and pin 4. The bus bar and resonator models each have an ETP, which is connected to the TRM. In a simulation, the dissipated powers in the bus bar and resonator are calculated and fed into the TRM, which represents the thermal behavior of the layout. The temperature value is calculated and fed back to the resonator in which the electrical response is adjusted due to the temperature-sensitive behavior (see Section IV-A). In the iterative simulation, a steady-state solution is derived. In sum, the RF response and the temperatures of both resonator and bus bar are simulated. This simulation model can be examined with arbitrary input signals. For the purpose of verification, a continuous wave (CW) sweep is utilized.

V. VERIFICATION EXPERIMENTS USING A TEMPERATURE SENSOR

Due to a relatively small area in the investigated design, the dissipated power densities in the series resonators SER3 and SER4 are relatively high compared to the remaining resonators. To verify the electrothermal simulation model, a resistive temperature sensor is implemented in the layout of the filter test structure at the resonator SER3. It is calibrated over temperature using a temperature-controlled wafer chuck.

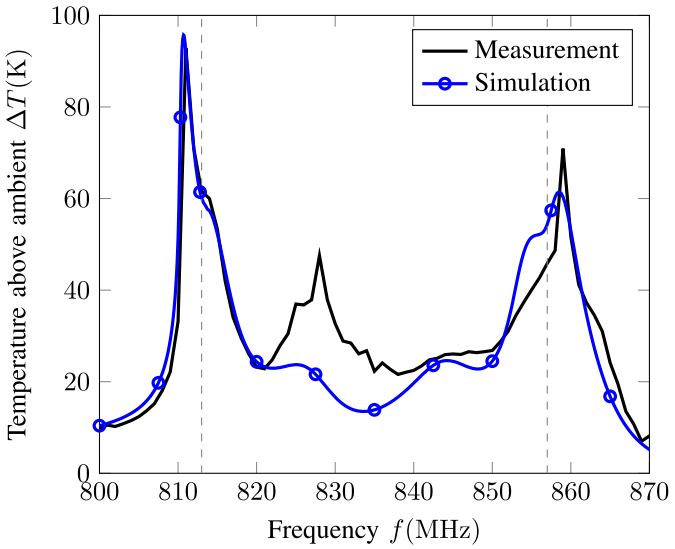

Fig. 10. Measured and simulated temperature increases of the series resonator SER3 in the filter test structure. The passband lies between the frequencies 813 and 857 MHz and is denoted with dashed lines.

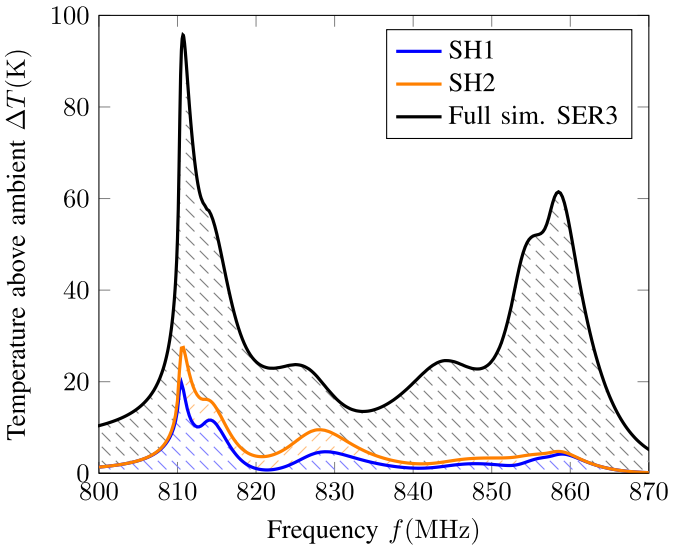

Fig. 11. Temperature increase of the resonator Ser3 and the impact of the two neighboring resonators (SH1 and SH2).

The sensor is connected via a dc probe, while the SAW filter test structure is excited with a high-power RF signal using two RF probes. A CW load tone at a power level of 29 dBm is applied to the test structure and swept between $f = 800$ MHz and $f = 870$ MHz in steps of 1 MHz. A vector network analyzer is used in a coupled path to check that a proper electrical connection is achieved. The large-signal input signal leads to frequency-dependent heating of the resonators and bus bar traces, which causes a temperature distribution across the filter layout. Naturally, each resonator's electrical response alters relatively to the gained temperature due to the TCF. This dynamic effect is considered in the developed electrothermal model. A comparison between measurement and simulation of the temperature increase at the resonator SER3 is shown in Fig. 10. The thermal simulation model is created using an experimentally determined $\kappa_{\text{Sub}} = 3.2$ (W/m · K). The remaining properties are based on thermal bulk material properties.

At the lower filter skirt, a maximum temperature increase of 92.8 K is measured at $f = 811$ MHz. The corresponding simulated maximum value is $\Delta T = 95.7$ K at a frequency of 810.7 MHz. At the upper filter skirt, the maximum temperature increase of 70.9 K is measured at $f = 859$ MHz, which corresponds to a simulated value of $\Delta T = 61.5$ K at a frequency of 858.5 MHz. The decay of temperature to frequencies below the lower filter skirt and above the upper skirt is well predicted. The deviation in the passband at $f = 828$ MHz can be explained by parasitic effects due to the touchdown of the dc probe that leads to a change in the filter transfer function. Considering the impact of the parasitic effect due to the dc probe, the measured and simulated responses show good agreement. Furthermore, a shift of the large-signal filter transfer function of 2 MHz at the lower skirt and 1 MHz at the upper skirt can be observed in comparison to a small-signal excitation. This dynamic effect is accurately represented by the electrothermal filter model.

VI. Simulation Using the Electrothermal Filter Model

The elaborated electrothermal model can be used to qualify the filter layout. Therefore, a simulation is run to evaluate the influence of the resonator SER3 due to the resonators SH1 and SH2. The simulated temperature increases are shown as a cumulative plot in Fig. 11.

The influence of mutual heating on the temperature increase of the resonator SER3 due to the resonator SH1 is highest at the frequency of 810.5 MHz. Its impact on ΔT is 19.7 K, which corresponds to 21.5% of the full temperature increase. The highest impact on the total temperature increase of SER3 is 24.6% at $f = 828.75$ MHz. At the upper filter skirt at $f = 859$ MHz, a contribution of 7.0% is observed. The mutual heating due to the resonator SH2 shows two peaks. At a frequency of 811 MHz, a $\Delta T = 9.7$ K is reached, which is a contribution of 10.6% to the resonator's SER3 temperature. At $f = 827$ MHz, a $\Delta T = 5.1$ K leads to 22.6% of the temperature increase of the resonator SER3. At higher frequencies, the impact is decreasing.

Based on this simulation, further decisions can be made on how to change the filter layout if temperature-related design goals are not met. For instance, a change in bus bar width, material stack, and the position of the individual resonators are possible starting points to improve the design.

VII. Conclusion

This article presents a derivation of an electrothermal modeling procedure for SAW filters and resonators. The thermal modeling in FEM is enabled by the elaboration of simplifications on the IDT and filter level. Therefore, an approach of equivalent 2-D layers to describe small 3-D objects and layer stacks is created. The complexity of the simulation model is drastically reduced, while the accuracy is hardly affected. The resulting TRM is implemented in a circuit simulator, and a dynamic full filter electrothermal model is set up. The comparison between the measurement of a filter test structure and a simulation model verifies the approach. Finally,

an exemplary simulation of the influence of mutual heating on the temperature increase of a series resonator is performed that can be used to improve the filter layout.

ACKNOWLEDGMENT

This article originates from a collaboration between the Institute for Electronics Engineering, Friedrich-Alexander University Erlangen-Nuremberg, and the company Qorvo. The authors would like to thank Jan H. Kuypers, Kimmo Kokkonen, Andreas Tag, Michael Fattinger, Sebastian Hübner, and Robert Aigner for their support, constructive discussions, and feedback.

REFERENCES

[1] B. Thomas, "White paper: Is your handset RF ready for 5G?" Qorvo, Greensboro, NC, USA, Tech. Rep. 1, Feb. 2018. [Online]. Available: https://www.qorvo.com

[2] T. Gillenwater, "Evolution of the smartphone," *Microw. J.*, vol. 60, pp. 1–5, Feb. 2017.

[3] P. Warder and D. Schnaufer, "Temperature-compensated filter technologies solve crowded spectrum challenges," *Microw. J.*, vol. 57, no. 11, pp. 90–98, Nov. 2014.

[4] K.-Y. Hashimoto, "Advances in RF SAW devices: What are demanded?" in *Proc. Eur. Freq. Time Forum (EFTF)*, Apr. 2016, pp. 1–4.

[5] O. Wunnicke, P. J. van der Wel, R. C. Strijbos, and F. de Bruijn, "Thermal behavior of BAW filters at high RF power levels," *IEEE Trans. Ultrason., Ferroelectr., Freq. Control*, vol. 56, no. 12, pp. 2686–2692, Dec. 2009.

[6] R. Aigner, G. Fattinger, M. Schaefer, K. Karnati, R. Rothemund, and F. Dumont, "BAW filters for 5G bands," in *IEDM Tech. Dig.*, Dec. 2018, pp. 14.5.1–14.5.4.

[7] R. Aigner and G. Fattinger, "3G–4G–5G: How baw filter technology enables a connected world," in *Proc. 20th Int. Conf. Solid-State Sens., Actuators Microsyst. Eurosensors*, Jun. 2019, pp. 523–526.

[8] M. Fattinger, P. Stokes, and G. Fattinger, "Thermal modeling of WLP-BAW filters: Power handling and miniaturization," in *Proc. IEEE Int. Ultrason. Symp. (IUS)*, Oct. 2015, pp. 1–4.

[9] A. Tag *et al.*, "Influence of temperature distribution on behavior, modeling, and reliability of BAW resonators," in *Proc. IEEE Int. Rel. Phys. Symp.*, Jun. 2014, pp. 5C.5.1–5C.5.7.

[10] C. Kirkendall and B. Ivira, "A hybrid 3D thermal/1D piezoelectric finite element model for rapid simulation of FBAR filter response under high power," in *Proc. IEEE Int. Ultrason. Symp. (IUS)*, Oct. 2018, pp. 1–6.

[11] A. G. Kozlov, "Modeling of thermal processes in thin-film BAW resonators," in *Proc. 20th Int. Conf. Thermal, Mech. Multi-Phys. Simulation Exp. Microelectron. Microsyst. (EuroSimE)*, Mar. 2019, pp. 1–8.

[12] V. Chauhan, C. Huck, A. Frank, W. Akstaller, R. Weigel, and A. Hagelauer, "Enhancing RF bulk acoustic wave devices: Multiphysical modeling and performance," *IEEE Microw. Mag.*, vol. 20, no. 10, pp. 56–70, Oct. 2019.

[13] A. Tag *et al.*, "A method for accurate modeling of BAW filters at high power levels," *IEEE Trans. Ultrason., Ferroelectr., Freq. Control*, vol. 63, no. 12, pp. 2207–2214, Dec. 2016.

[14] M. Gonzalez-Rodriguez, J. Mateu, C. Collado, J. M. Gonzalez-Arbesu, and R. Aigner, "Analytical modeling method of thermal spreading resistance in BAW filters," in *Proc. IEEE Int. Ultrason. Symp. (IUS)*, Oct. 2019, pp. 1707–1710.

[15] S. Setoodeh, U. Kemiktarak, F. Bayatpur, S. Fouladi, and D. Feld, "A high power circuit model of an FBAR resonator for use in filter design," in *Proc. IEEE Int. Ultrason. Symp. (IUS)*, Oct. 2019, pp. 2169–2173.

[16] J. Segovia-Fernandez and G. Piazza, "Thermal nonlinearities in contour mode AlN resonators," *J. Microelectromech. Syst.*, vol. 22, no. 4, pp. 976–985, Aug. 2013.

[17] R. Lu and S. Gong, "Study of thermal nonlinearity in lithium niobate-based MEMS resonators," in *Proc. 18th Int. Conf. Solid-State Sens., Actuators Microsystems (TRANSDUCERS)*, Jun. 2015, pp. 1993–1996.

[18] K. Gamble and W. Buettner, "Steady-state and transient thermal modeling for a SAW duplexer," in *Proc. IEEE Int. Ultrason. Symp. (IUS)*, Sep. 2016, pp. 1–6.

[19] J. Costa *et al.*, "Design and characterization of SAW filters for high power performance," in *Proc. IEEE Int. Ultrason. Symp. (IUS)*, Sep. 2017, pp. 1–4.

[20] I. N. Bronstein, K. A. Semendjajew, G. Musiol, and H. Mühlig, *Taschenbuch der Mathematik*, 2nd ed. Frankfurt, Germany: Verlag Harri Deutsch, 2001.

[21] N. B. Hassine *et al.*, "Self heating under RF power in BAW SMR and its predictive 1D thermal model," in *Proc. IEEE Int. Freq. Control Symp. Joint 22nd Eur. Freq. Time Forum*, Apr. 2009, pp. 237–240.

[22] Y. A. Cengel and A. J. Ghajar, *Heat and Mass Transfer: Fundamentals and Applications*. New York, NY, USA: McGraw-Hill, 2015.

[23] J. P. Dunsmore, *Handbook of Microwave Component Measurements: With Advanced VNA Techniques*, 2nd ed. Hoboken, NJ, USA: Wiley, Sep. 2012.

[24] W. Akstaller, R. Weigel, A. Hagelauer, J. Kuypers, and K. Kokkoncn, "Electro-thermal modeling of TCSAW filter," in *Proc. IEEE Int. Ultrason. Symp. (IUS)*, Oct. 2018, pp. 1–4.

Wolfgang Akstaller (Student Member, IEEE) received the B.Sc., M.Sc., and Dr.-Ing. degrees in electrical engineering from Friedrich-Alexander-University Erlangen-Nurember, Erlangen, Germany, in 2013, 2014, and 2019, respectively.

From 2015 to 2018, he was a Scientific Researcher at the Institute for Electronics Engineering, Friedrich-Alexander-University Erlangen-Nuremberg, with a focus on thermal and nonlinear electrical characterization, modeling and simulation of microacoustic SAW devices. He is currently working on microwave-based sensor systems.

Robert Weigel (Fellow, IEEE) was born in Ebermannstadt, Germany, in 1956. He received the Dr.-Ing. and Dr.-Ing.habil. degrees in electrical engineering and computer science from the Munich University of Technology, Munich, Germany, in 1989 and 1992, respectively.

He was a Research Engineer, a Senior Research Engineer, and a Professor for RF Circuits and Systems with the Munich University of Technology until 1996. From 1994 to 1995, he was a Guest Professor for SAW Technology at Vienna University of Technology, Vienna, Austria. From 1996 to 2002, he has been the Director of the Institute for Communications and Information Engineering, University of Linz, Linz, Austria, where he co-founded the company DICE, Linz, in August 1999, meanwhile split into an Infineon Technologies (DICE) and an Intel (DMCE) company which are devoted to the design of RFICs for mobile radio and MMICs for vehicular radar applications. In 2000, he has been appointed a Professor for RF Engineering at the Tongji University, Shanghai, China. Since 2002, he has been the Head of the Institute for Electronics Engineering, University of Erlangen-Nuremberg, Erlangen, Germany. There, respectively in 2009, 2012, and 2015, he co-founded the companies eesy-id, Gräfelfing, Germany, eesy-ic, Erlangen, and eesy-innovation, Unterhaching, Germany. He has been engaged in research and development of microwave theory and techniques, electronic circuits and systems, and communication and sensing systems. In these fields, he has authored or coauthored more than 900 articles.

Dr. Weigel is an Elected Member of the German National Academy of Science and Engineering (acatech) and the Senate of the German Research Foundation (DFG). He received the 2002 VDE ITG-Award, the 2007 IEEE Microwave Applications Award, and the 2016 IEEE MTT-S Distinguished Educator Award. He is and has been serving on numerous advisory boards of government bodies, research institutes, and companies in Europe and Asia. Furthermore, he is and has been serving on various editorial boards such as that of the PROCEEDINGS OF THE IEEE. He also has been Founding Editor of the Proceedings of the European Microwave Association (EuMA) which in 2008 where transformed into EuMAs *International Journal of Microwave and Wireless Technologies*. He has been a member of numerous conference steering and technical program committees. He was a General Chair of several conferences such as the 2013 European Microwave Week in Nuremberg, Germany, and Technical Program Chair of several conferences such as the 2002 IEEE International Ultrasonics Symposium in Munich. He served in many roles for the IEEE MTT and UFFC Societies. He has been Founding Chair of the Austrian COM/MTT Joint Chapter, Region 8 MTT-S Coordinator, Distinguished Microwave Lecturer, MTT-S AdCom Member, and the 2014 MTT-S President.

Amelie Hagelauer (Senior Member, IEEE) received the Dipl.Ing. degree in mechatronics and the Dr.Ing. degree in electrical engineering from Friedrich-Alexander University Erlangen-Nuremberg, Erlangen, Germany, in 2007 and 2013, respectively.

She joined the Institute for Electronics Engineering, Friedrich-Alexander University Erlangen-Nuremberg, in November 2007, where she was involved in thin-film BAW filters. Since 2013, she has been focusing on SAW/BAW and RF MEMS components, as well as integrated circuits for front ends up to 180 GHz. She has been a Professor with Universitat Bayreuth, Bayreuth, Germany, since August 2019.

Dr. Hagelauer was the Chair of MTT-2 Microwave Acoustics from 2015 to 2017. She is continuously contributing to the development of the RF Acoustics community by organizing workshops and student design competitions. She has been acting as an Associate Editor of the IEEE TRANSACTIONS ON MICROWAVE THEORY AND TECHNIQUES, as a Guest Editor for a Special Issue of the IEEE TRANSACTIONS ON MICROWAVE THEORY AND TECHNIQUES on the topic RF Front ends for Mobile Radio and for a Special Issue in the *MDPI Journal Sensors* on the topic Surface Acoustic Wave and Bulk Acoustic Wave Sensors.